
Article:
Bonilla Licea, D, Zaidi, SAR, McLernon, D et al. (1 more author) (2016) Improving Radio Energy Harvesting in Robots using Mobility Diversity. IEEE Transactions on Signal Processing, 64 (8). pp. 2065-2077. ISSN 1053-587X

https://doi.org/10.1109/TSP.2016.2518999

Improving Radio Energy Harvesting in Robots using Mobility Diversity

Daniel Bonilla Licea, Syed Ali Raza Zaidi, Des McLernon and Mounir Ghogho

***Abstract*—In this article, we propose a new technique which exploits a robot's (intelligently) controlled mobility to maximise stored radio energy. In particular, we examine a scenario where the mobile robot takes a break from its normal activity for a duration of T secs. This 'dead time' consists of three phases - searching, positioning and resting - which ensure that the robot can optimise its energy harvesting from a base station transmitting a narrowband RF signal over a flat fading wireless channel. We utilise the mobility diversity principle, which arises due to the spatial wireless channel diversity experienced by motion of the robot. By optimal exploitation of the small scale fading we maximize the net amount of energy (i.e., the energy harvested by the robot minus the mechanical energy used for motion) that the robot stores over the 'dead time'. To the best of the authors' knowledge, this article is the first use of the mobility diversity principle to optimise energy harvesting from an RF signal. We demonstrate that mobility, if intelligently controlled, is actually not a foe but is indeed a friend which can provide significant benefits under wireless fading channels. Through simulations we verify the analytical results and illustrate the improvement in the energy stored compared with not using intelligent mobility. Finally, we show that the efficiency of our approach is clearly coupled with various design parameters including the centre frequency of the narrowband RF signal and the duration of the 'dead time'.**

***Index Terms*—mobility diversity; energy harvesting; optimal control; fading; mobile robot.**

I. Introduction

A. Motivation

MOBILITY and fading are traditionally regarded as foes in the context of wireless communication. Both phenomena manifest frequent variations in the propagation channel, causing transmission outages. Recently, it was demonstrated that for delay tolerant applications, mobility can be exploited to harness capacity gains in wireless ad-hoc networks [1]. Nevertheless, the focus has been to exploit mobility to diminish co-channel interference by reducing the effective number of transmissions. A natural, and more intelligent approach, would be to complement interference reduction with optimal exploitation of the intrinsic diversity offered under node mobility. More recently, it was shown [2] that in the context of applications where mobility can be controlled, channel-aware trajectory planners [3] can be devised to harness the intrinsic diversity gain. Communications for mobile robotic platforms is one such application that can avail of such a concept.

Mobile robots (MRs) are currently of great interest to both the academic research community and industry. This can be attributed to the associated wide spectrum of applications (e.g. health care [4], rescue [5], [6], [7], construction [8], exploration [9], surveillance [10] and entertainment [11] among many others) as well as its interdisciplinary nature involving communications [12], [13], [14], control and embedded systems.

Untethered MRs draw their energy exclusively from an onboard battery. The amount of tasks the MR can execute depends on the energy stored in its battery. Hence energy, in the context of untethered MRs, is a very scarce and important resource. There are many approaches that allow the robots to increase the time duration over which an untethered MR can operate without having to return to its base for recharging its battery. These include using energy conservation techniques to make the robot more energy efficient [15] or adding energy harvesting capabilities to the MR [16], [17]. Now, wireless energy harvesting [18] is a technique that is being studied with applications to sensor networks but it could be applied to small untethered MRs requiring low power. This can be done by using a dedicated base station (BS) to transmit RF energy and adding a rectifier antenna [19] to the MR so that it stores the wireless energy transmitted by the BS. Although the amount of energy stored by this method may not be as high as with other energy harvesting techniques (e.g., solar or wind energy) it is cheap to implement and it requires only a very small area on the robot's surface. Because of this latter property wireless energy harvesting systems can easily be implemented on small MRs (e.g. the micro-robot Alice [20], [16]). Moreover, the key advantage in RF energy harvesting is that it imposes minimal hardware requirements for MRs, as they are already provided with on-board radio communication capabilities.

B. Problem Overview

In this article, we consider an untethered MR with an antenna which uses the integrated receiver architecture presented in [21] that provisions simultaneous data and wireless energy reception from the command-and-control center BS. This BS is charged to maintain communications for control purposes or just to exchange data with the MR. More specifically, we consider a scenario where a MR, that is harvesting wireless

Daniel Bonilla Licea is with the University of Leeds, UK, e-mail:eldbl@leeds.ac.uk. The author acknowledges the funding of CONACYT, Mexico.

Des McLernon is with the University of Leeds, UK, e-mail: d.c.mclernon@leeds.ac.uk.

Mounir Ghogho is with the University of Leeds, UK and the International University of Rabat, Morocco, e-mail: m.ghogho@ieee.org.

Syed Ali Raza Zaidi is with the University of Leeds, UK, e-mail: s.a.zaidi@leeds.ac.uk.

energy most of the time[1] thanks to the receiver mentioned earlier, is deployed in the field. The robot has to perform a series of tasks demanded by the BS. Now, we assume that there are 'dead times' between the tasks which are demanded by the BS. This means that once the MR completes one task it will not be required to perform any further action for a 'dead time' of duration T seconds until the BS request execution of the next task. During the execution of a task the MR will harvest wireless energy while completing it.

During the 'dead times' the BS transmits an RF signal so that the MR can harvest energy from it. Generally, MRs may observe many scatterers in their near vicinity and that there may not be a line of sight between the MR and the BS antenna. Therefore, the wireless channel from the BS to the MR will experience small scale fading which will affect the amount of radio energy that can be harvested. Thus, the key challenge posed in this scenario is to devise a MR algorithm which maximizes the energy stored during these 'dead times' in the presence of fading. What should the MR do during these 'dead times' in order to maximize the amount of energy stored over that period? Should the MR just stand still and continue harvesting wireless energy? The purpose of this article is to answer these questions and derive an optimal algorithm for the MR to execute during the 'dead times'. In order to solve this problem, we propose to exploit the so called 'mobility diversity principle' [2], [12] to take advantage of the wireless channel fading by using the motion of the MR.

The mobility diversity principle (i.e., exploiting the MR motion to combat small scale fading) is quite a recent idea. In [12] the authors demonstrated that moving the robot can considerably improve the propagation conditions. The authors proposed several mobility strategies and coined the term 'RF Mobility Gain'. In [13], the authors designed a mobility controller in order to maximize the channel capacity between the MR and a BS under Rayleigh fading while satisfying some tracking constraints for a certain pre-defined trajectory. In [14], they considered a scenario where the robot explores and measures the channel gains at N points which are randomly distributed in a circular area. Following the exploration and measurement phase, the robot then moves to the location with the highest channel gain and transmits from that point.

While the above-mentioned articles highlight the optimal exploitation of controlled mobility, they did not consider the mechanical energy used by the robot in attaining these optimal operating points. So the authors in [2] devised a mobility control strategy such that a MR operating in a fading environment can locate an optimal transmitting position; the proposed approach relies on calculating the stopping points which a robot has to explore in order to find the best transmitting position. However, as opposed to [14], in [2] the geometry of the stopping points was optimized by considering the spatial correlation function of the wireless channel while using a model where the energy consumed is proportional to the distance travelled by the robot. In articles [3] and [22], the authors employed the channel spatial correlation function and devised an iterative "trajectory planner" which finds a stopping point with a high channel gain in order to minimize the power required for successful transmission. The authors in [3] and [22] also considered the mechanical energy consumed by the robot.

The mobility technique proposed in this study differs from all the above-mentioned approaches ([2]-[22]) in two specific aspects:

1) *Application*: The previous literature has focused on optimal "trajectory planning" to find the best position for transmitting data from the MR to the BS such that the energy required for this operation is minimized. However, this paper is geared towards determination of the optimal motion on a path such that the net amount of energy stored during 'dead times' (i.e., the radio energy harvested minus the mechanical energy consumed for the spatial exploration) is maximized. The key difference is that in the previous literature the energy used for wireless transmission depends only on the position of the points where the channel is measured. But in this paper, the net energy stored due to harvesting depends both on the position of the points where the channel is measured and the temporal duration of the 'dead time'. So we have added the temporal dimension in this problem.
2) *Modeling*: Another difference between the existing literature and this paper is the model employed for the MR. The mathematical model of the MR dictates its mechanical energy consumption and so it is important to have a good model. In [2], [3] and [22], the authors considered a simple model for a MR and assumed that its mechanical energy consumption is proportional to the distance traveled. However, in this paper, we consider a more comprehensive and realistic model. Here, we only consider a linear movement[2] for the robot (as in [12]) during the 'dead times' but in contrast to [12], we are able to optimize analytically the length of the line to be explored.

C. Contribution & Organization

The main contribution of this paper is to demonstrate the fact that the optimal behaviour to maximize the energy stored (in presence of fading) during the 'dead times' is not to simply stand still but to move intelligently. Another contribution is the utilization and optimization (using joint communications and control concepts) of the mobility diversity principle for the problem of radio energy harvesting. In particular, we will show that by moving in an optimized way we can increase (on average) the amount of energy stored by the robot (i.e., the radio energy harvested minus the mechanical energy consumed for the exploration). Finally, as we will show in the next sections, this technique assumes that over the period when the robot is stationary, the wireless channel is time-invariant.

[1]The only times when the MR is not harvesting wireless energy could be when the it is transmitting. This is because at that time the antenna could be connected to the transmitter instead of the receiver (depending on the transceiver architecture.)

[2]Note that only linear movement is currently considered because comprehensive and accurate analytical results (i.e., the mathematics is tractable) can then be derived from the MR model under such a restricted trajectory. Nevertheless other types of movement merit investigation in future works.

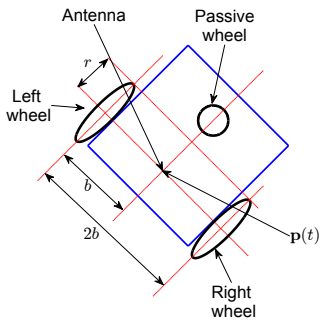

Figure 1. Diferential drive robot (DDR).

This implies highly "stationary" physical environments and so our approach is suitable for applications such as surveillance museums at night or cave exploration.

This paper is now organized as follows. In section II we describe the models for the robot, for the channel and for the energy storage system. Then in section III we propose an energy harvesting technique which makes use of the mobility diversity principle. In section IV we optimize the parameters of this technique. An explanation about how to find the optimal point from which to harvest the energy is presented in section V. Finally, simulation results are given in section VI and conclusions are presented in section VII.

D. Notation

The first and second time derivatives of $x(t)$ are $\dot{x}(t)$ and $\ddot{x}(t)$ respectively. The superscript T represents the transpose matrix while the superscript $-T$ represents the transpose of the inverse matrix. The Euclidian norm of a vector is written $\|\cdot\|_2$, and the expected value is $\mathbb{E}[\cdot]$. Finally $\mathcal{R}(\sigma)$ represents the Rayleigh distribution with standard parameter σ and $\lceil x \rceil$ is the ceil function.

II. System and Channel Model

The objectives of this section are the following:

1) To present the model for the MR. We will briefly summarize the dynamics and the associated parameters of the MR which contribute towards it mechanical energy consumption.
2) To discuss the channel model for the link used to transmit electromagnetic energy from the BS to the MR.
3) To briefly describe the energy storage system model.

A. MR Model

In this article, we consider a MR and in particular we assume a differential drive robot[3] (DDR) [25] furnished with a rectifier antenna[4] (rectenna) [19]. It is assumed that the rectenna is installed on the geometric center of the robot (see Fig. 1) such that it can harvest the energy received from the BS located at the 2-D point, $\mathbf{p}_{BS}$. A DDR is a MR that has two wheels (each with radius r controlled by its own motor). The distance between the two motorized wheels is $2b$. In addition, it may have a third passive[5] omnidirectional[6] wheel which serves as support for the robot (see Fig. 1). The DDR model considered in this article is a version of the model presented in [27].

The position of the MR is $\mathbf{p}(t)$ and its translational velocity $v(t)$ is controlled by the motor's input vector $\mathbf{u}(t) = [u^R(t) \quad u^L(t)]^T$ where $u^R(t)$ and $u^L(t)$ are the control inputs for the right and left motors respectively. The following state equation describes how $v(t)$ is controlled by $\mathbf{u}(t)$:

$$\dot{v}(t) + [1 \quad 0]\bar{\mathbf{A}}[v(t) \quad 0]^T = [1 \quad 0]\bar{\mathbf{B}}\mathbf{u}(t), \tag{1}$$

where $\bar{\mathbf{A}} = c_A \mathbf{T_q} \mathbf{J}^{-1} \mathbf{T_q}^{-1}$ and $\bar{\mathbf{B}} = c_B \mathbf{T_q} \mathbf{J}^{-1}$, with c_A and c_B two constants depending on the electromechanical characteristics of the robot (see [27]); the matrix $\mathbf{J}$ is the equivalent inertia matrix of the robot's motors (see [27]):

$$\mathbf{J} = \begin{bmatrix} J_1 & J_2 \\ J_2 & J_1 \end{bmatrix}, \tag{2}$$

and $\mathbf{T_q}$ depends on the geometry of the robot and is given by:

$$\mathbf{T_q} = \begin{bmatrix} r/2 & r/2 \\ r/2b & -r/2b \end{bmatrix}. \tag{3}$$

Finally, the energy consumed by the MR due to its mechanical movement from any time t_0 to time t_1 is [27]:

$$\begin{aligned} E_{mech}(\mathbf{u}(t), t_0, t_1) &= \int_{t_0}^{t_1} c_1 \mathbf{u}^T(t)\mathbf{u}(t)\mathrm{d}t \\ &- \int_{t_0}^{t_1} c_2 [v(t) \quad 0]\mathbf{T_q}^{-T}\mathbf{u}(t)\mathrm{d}t, \end{aligned} \tag{4}$$

where c_1 and c_2 are constants which depend on the electrical parameters of the robot's motors.

B. Channel Model

In this article, we consider that during the dead time of duration T the BS is constantly transmitting a narrowband RF signal $e_{RF}(t)$ so that the robot can replenish its battery with RF harvested energy. A narrowband signal will produce less interference to adjacent wireless systems than a broadband signal. Now while narrowband signals will experience flat fading, which in turn will produce losses[7] in the wireless energy harvested by the system, this impairment will be compensated through the MR movement (as we will see later in the article).

Now, we assume that the MR receiver follows the architecture proposed in [21]. On the MR, the energy is received by a rectenna. The output of the rectifier is connected to both the robot's battery and an analog-to-digital converter (ADC) (see Fig. 2). In general, the receiver in Fig. 2 serves to receive information (through the ADC) while simultaneously

[3]Although we restrict our analysis to a DDR the technique presented in this article can be easily extended to other types of MR like (for example) a three wheeled omni-directional robot [23] which uses the model in [24].

[4]An antenna which is connected directly to a rectifier composed of a Schottky diode and a lowpass filter. This kind of antenna is used in practical energy harvesting systems [26].

[5]A passive wheel is a wheel which is not controlled by any motor.

[6]An omnidirectional wheel can roll in any direction at any time.

[7]Due to the deep fades.

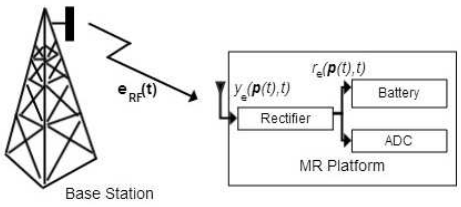

Figure 2. Energy receiver architecture [21].

harvesting radio energy, but during the dead times the receiver will just be used to harvest radio energy. We also assume that most of the energy generated at the output of the rectifier is fed to the battery and only a small amount is absorbed by the ADC's input. This may be achieved by inserting (at the rectifier's output) a well-designed three-port matching network [28] (not shown in Fig. 2) with one input and two outputs. Consequently, the on-board battery is charged by employing the radio signal, while the MR simultaneously monitors the amount of energy that arrives into its battery.

Since the radio signal transmitted by the BS is narrow band the wireless channel experiences flat fading. Furthermore, it is assumed that during the dead time the environment remains stationary and consequently the duration T of the dead time is smaller than the coherence time of the channel and so the channel will be considered approximately time-invariant over this duration. Note that this can only be achieved if the MR works on environments with physical features that experience low mobility. So the low-pass, complex equivalent baseband signal received by the robot's antenna at position $\mathbf{p}(t)$ is given by

$$y_e(\mathbf{p}(t),t) = \frac{s(\mathbf{p}(t)) \cdot h(\mathbf{p}(t))}{\|\mathbf{p}(t) - \mathbf{p}_{BS}\|_2^{\gamma/2}} e(t) + n_y(t), \tag{5}$$

where $n_y(t) \sim \mathcal{CN}(0, \sigma_y^2)$ is complex, zero-mean, additive white Gaussian noise (AWGN), $s(\mathbf{p}(t))$ is the shadowing experienced at the position $\mathbf{p}(t)$, $h(\mathbf{p}(t))$ is the small-scale fading observed at $\mathbf{p}(t)$, $\gamma \geq 2$ is the environment dependent path-loss coefficient and $e(t)$ is the lowpass equivalent of a pure RF tone $e_{RF}(t)$ with amplitude g.

If the movement of the robot during the dead times is in a small region then we have that $s(\mathbf{p}(t)) = s_0$, a constant, i.e., the shadowing term is constant for all the positions in which the robot moves during the dead times. In addition, if that region is also small with respect to the distance to the BS, then we can say that during the dead times we have $\|\mathbf{p}(t) - \mathbf{p}_{BS}\|_2 \approx \|\mathbf{p}(0) - \mathbf{p}_{BS}\|_2 = \|\mathbf{p}_{BS}\|_2$. With all these considerations then (5) simplifies to:

$$y_e(\mathbf{p}(t),t) = h(\mathbf{p}(t)) \cdot g_y + n_y(t), \tag{6}$$

where $g_y = g \cdot s_0 \cdot \|\mathbf{p}_{BS}\|_2^{-\gamma/2}$. We will consider that the small scale fading follows Jake's model [29] and so $|h(\mathbf{p}(t))| \sim \mathcal{R}\left(\frac{1}{\sqrt{2}}\right)$ is Rayleigh distributed and the normalized spatial covariance function of the channel gain is:

$$\begin{aligned} C(\mathbf{p},\mathbf{q}) &= \frac{4\mathbb{E}[(|h(\mathbf{p})| - \mathbb{E}[|h(\mathbf{p})|])(|h(\mathbf{q})| - \mathbb{E}[|h(\mathbf{q})|])]}{(4-\pi)}, \\ &= J_0^2\left(\frac{2\pi\|\mathbf{p}-\mathbf{q}\|_2}{\lambda}\right), \end{aligned} \tag{7}$$

where λ is the wavelength of the RF signal transmitted by the BS and $J_0(x) = {}^1\!/_\pi \int_0^\pi \cos(x\sin(\theta))d\theta$ is a zero-order Bessel function of the first kind. The signal at the output of the rectifier in Fig. 2 is [21]:

$$r_e(\mathbf{p}(t),t) = g_e|y_e(\mathbf{p}(t),t)|^2 + n_r(t), \tag{8}$$

where g_e is the gain of the rectifier (without any loss of generality we will assume $g_e = 1$) and $n_r(t) \sim \mathcal{N}(0, \sigma_r^2)$ is the real, zero-mean, AWGN at the output of the rectifier. We will refer to $n_r(t)$ as the post-rectifier noise and to $n_y(t)$ in (5) as the pre-rectifier noise in order to differentiate between them. Finally, the signal at the output of the ADC can be characterised as $r_e(\mathbf{p}(k\Delta_s), k\Delta_s)$ with $k\Delta_s$ being the discrete sampling time. We will use $r_e(k)$ as the shorthand notation for $r_e(\mathbf{p}(k\Delta_s), k\Delta_s)$, and the same reasoning will apply for all the discrete-time signals in the rest of this article.

C. Energy Storage System

The energy storage system is a vital component of the DDR. The net amount of energy stored from any time t_0 to t_1 can be written as

$$E_s(t_0,t_1) = E_r(\mathbf{p}(t),t_0,t_1) - E_{mech}(\mathbf{u}(t),t_0,t_1), \tag{9}$$

where $E_r(\mathbf{p}(t),t_0,t_1)$ is the energy harvested over this time period using the rectenna. Mathematically, this can be written as:

$$E_r(\mathbf{p}(t),t_0,t_1) = \eta \int_{t_0}^{t_1} r_e(\mathbf{p}(\tau),\tau)d\tau, \tag{10}$$

where $\eta \in (0,1]$ is the energy charging efficiency parameter [30]. The energy storage efficiency of the robotic platform depends on the impedance matching network at the rectifier's output and also on the energy charging system for the battery. Although the battery has finite capacity we will not consider this on our model because we assume that the amount of energy stored in the battery at the beginning of the dead time is not high enough so that the battery can be completely replenished at the end of this period. In the same manner, we will assume that the battery level at the beginning of the dead time is not low enough so that the MR runs out of energy because of the motion carried out during this period of time.

III. Proposed MR Energy Harvesting Technique (MR-EHT)

As we will define later in this section, the dead time of T secs (from $t = 0$ to $t = T$) when the MR is attempting to find an optimal position from which to "re-energize" itself, will comprise of three phases. Only during the third phase will the MR actually be stationary. The objective is to maximise $\mathbb{E}[E_s(0,T)]$ in (9). Now, due to the small scale fading, the radio energy harvested by the MR using its rectenna can be

very low if the MR is located at a position where the channel gain is poor. Nevertheless, although in principle the fading seems to be a problem, it can be exploited by optimally controlling the mobility of the robot to find a position with high channel gain. In other words, we shall use the mobility diversity principle [2] to maximize the energy stored by the MR during the dead time.

During the dead time, the more points the robot explores the higher is the probability of finding a point with a high channel gain and so increasing the radio energy harvested $E_r(\mathbf{p}(t), 0, T)$. Nevertheless, performing this exploration demands significant mobility which comes at the expense of mechanical energy consumption, see (4). This mechanical energy consumption in turn depletes the energy from the MR's battery. This implies that although moving can significantly increase $E_r(\mathbf{p}(t), 0, T)$ it also increases $E_{mech}(\mathbf{u}(t), 0, T)$ and consequently the net energy $E_s(0, T)$ (see (9)) can be low or even negative. This encourages intelligent mobility control such that the energy stored during the dead time is maximized. In short, in the RF energy harvesting problem for MRs the net energy stored is highly dependent on the actual exploration strategy.

So first of all we define the design parameters $T_s < T$ and $\alpha \in (0, 1)$, which will be optimized in section IV. We propose that the dead time is divided into three distinct phases:

1) **Phase 1 - Searching Time** ($t \in [0, \alpha T_s]$) During this period the MR moves into a search space while simultaneously monitoring the channel gain and harvesting energy.
2) **Phase 2 - Positioning Time** ($t \in (\alpha T_s, T_s]$) During this phase the MR continues harvesting energy while moving from its current location $\mathbf{p}(\alpha T_s)$ to the optimal operating point $\hat{\mathbf{p}}_{opt}$, where $\hat{\mathbf{p}}_{opt}$ is the estimation of $\mathbf{p}_{opt}$ defined as:
$$\mathbf{p}_{opt} = \arg \max_{\substack{\mathbf{p}(t) \\ t \in [0, \alpha T_s]}} |h(\mathbf{p}(t))|. \quad (11)$$
3) **Phase 3 - Resting Time** ($t \in (T_s, T]$) In this period the robot remains motionless at $\hat{\mathbf{p}}_{opt}$ harvesting energy through its rectenna.

Following (9) the net energy stored during the harvesting time (i.e., over the total pause period of T seconds) is:

$$\begin{aligned} E_s(0,T) &= \overbrace{E_r(\mathbf{p}(t),0,\alpha T_s) + E_r(\mathbf{p}(t),\alpha T_s, T_s)}^{\text{Harvested energy (Phases 1\& 2)}} \quad (12) \\ &+ \overbrace{E_r(\hat{\mathbf{p}}_{opt}, T_s, T)}^{\text{Harvested energy (Phase 3)}} \\ &- \underbrace{E_{mech}(\mathbf{u}_1(t),0,\alpha T_s) - E_{mech}(\mathbf{u}_2(t),\alpha T_s, T_s)}_{\text{Energy consumed due to mobility in Phases 1 \& 2}}. \end{aligned}$$

where $\mathbf{u}_1(t)$ and $\mathbf{u}_2(t)$ are the control inputs (see (1)) employed during the first and second phases[8]. Let us define the searching space (for phase 1) as the following set:

$$\mathcal{S} = \{\mathbf{q} \mid \mathbf{q} = \mathbf{p}(t) \quad \text{for} \quad t \in [0, T]\}. \quad (13)$$

[8]Note that energy is harvested during all three phases of the dead time but it is during phase 3 that the most significant harvesting actually takes place.

The selection of the optimal set $\mathcal{S}$ is an open problem and is outside of the scope of this article. So in this article, for simplicity of the trajectory planning of the MR, we will select a straight line of length L as the searching space:

$$\mathcal{S} = \{l\bar{\mathbf{v}} \mid \bar{\mathbf{v}} = [1 \;\; 0]^T, \; l \in [0, L]\}. \quad (14)$$

This implies that:

1) The control input $\mathbf{u}_1(t)$ has to follow a control law that takes the robot from its initial state $\mathbf{z}(0) = \mathbf{0}$ and initial pose $\mathbf{p}_o(0) = \mathbf{0}$ to the final state $\mathbf{z}(\alpha T_s) = \mathbf{0}$ and final pose $\mathbf{p}_o(\alpha T_s) = [L \;\; 0 \;\; 0]^T$ while moving in a straight line.
2) The control input $\mathbf{u}_2(t)$ has to follow a control law that takes the robot from the initial state $\mathbf{z}(\alpha T_s) = \mathbf{0}$ and initial pose $\mathbf{p}_o(\alpha T_s) = [L \;\; 0 \;\; 0]^T$ to the final state $\mathbf{z}(T_s) = \mathbf{0}$ and final pose $\mathbf{p}_o(T_s) = [\hat{\mathbf{p}}_{opt} \;\; 0 \;\; 0]^T$. Since $\mathbf{p}_{opt}$ and $\hat{\mathbf{p}}_{opt}$ are both random variables the control law $\mathbf{u}_2(t)$ is a stochastic process (as opposed to $\mathbf{u}_1(t)$ which is deterministic).

IV. Optimization of MR-EHT

In this section, our objective is to optimize the proposed MR-EHT so that the expected value of the net energy stored during the dead time is maximized. In other words, we want to maximize the average net stored energy $\mathbb{E}[E_s(0, T)]$. The optimization process will ensure that the average energy level of MR battery at the end of the dead time will be maximized.

For this section, we assume that $\mathbf{p}_{opt}$ is known and therefore $\hat{\mathbf{p}}_{opt} = \mathbf{p}_{opt}$ (In section V, we provide further details of the estimation process for $\mathbf{p}_{opt}$). Finally, we assume that we know g_y in (6), this term can be estimated by using the techniques described in [31] or [32].

Substituting (10) into (12) and applying expected value to (12) we obtain:

$$\begin{aligned} \mathbb{E}[E_s(0,T)] &= \eta \int_0^{\alpha T_s} \mathbb{E}[r_e(\mathbf{p}(\tau),\tau)]d\tau \\ &+ \eta \int_{\alpha T_s}^{T_s} \mathbb{E}[r_e(\mathbf{p}(\tau),\tau)]d\tau \\ &+ \eta \int_{T_s}^{T} \mathbb{E}[r_e(\mathbf{p}_{opt},\tau)]d\tau \\ &- E_{mech}(\mathbf{u}_1(t),0,\alpha T_s) \\ &- \mathbb{E}[E_{mech}(\mathbf{u}_2(t),\alpha T_s, T_s)]. \quad (15) \end{aligned}$$

We will now examine in turn each of the five terms on the RHS of (15). The first term corresponds to the energy harvested during the first phase we can easily demonstrate that:

$$\mathbb{E}[r_e(\mathbf{p}(\tau),\tau)] = g_y^2 + \sigma_y^2. \quad (16)$$

The second term on the RHS of (15) corresponds to the energy harvested during the second phase. In this phase the MR starts at position $\mathbf{p}(\alpha T_s)$ (which is a deterministic position) and finishes at $\mathbf{p}(T_s) = \mathbf{p}_{opt}$ (which is a random position). Now, $|h(\mathbf{p}(\alpha T_s))| \sim \mathcal{R}\left(\frac{1}{\sqrt{2}}\right)$ and so $\mathbb{E}[|h(\mathbf{p}(\alpha T_s))|^2] = 1$. Also, due to the definition of $\mathbf{p}_{opt}$ then, for $L > 0$, $\mathbb{E}[|h(\mathbf{p}(T_s))|^2] > 1$. During this phase, if at time instant t the

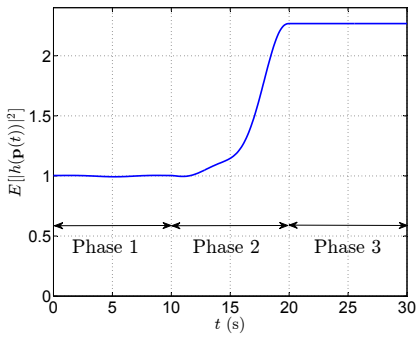

Figure 3. Evolution of $\mathbb{E}[|h(\mathbf{p}(t))|^2]$ during the execution of the three phases (see start of section III) with $T = 30$s, $T_s = 20$s, $\alpha = 0.5$ and $L = 1\lambda$.

MR is 'near' to $\mathbf{p}_{opt}$ then $h(\mathbf{p}(t))$ will be highly correlated with $h(\mathbf{p}(T_s)) = h(\mathbf{p}_{opt})$ and so $\mathbb{E}[|h(\mathbf{p}(t))|^2]$ will be just slightly inferior to $\mathbb{E}[|h(\mathbf{p}_{opt})|^2]$. On the other hand, if at time instant t the MR is 'far' from $\mathbf{p}_{opt}$ then $h(\mathbf{p}(t))$ will be almost uncorrelated with $h(\mathbf{p}(T_s)) = h(\mathbf{p}_{opt})$ and so $\mathbb{E}[|h(\mathbf{p}(t))|^2] \approx 1$. This all means that during this second phase $\mathbb{E}[|h(\mathbf{p}(t))|^2] > 1$ and $\mathbb{E}[|h(\mathbf{p}(t))|^2]$ increases from 1 to $\mathbb{E}[|h(\mathbf{p}_{opt})|^2]$. In Fig. 3 we illustrate with this temporal evolution with an example. A more detailed analysis of the behaviour of $\mathbb{E}[|h(\mathbf{p}(t))|^2]$ for this phase is outside the scope of this article but will be the subject of future work. These results imply that $\mathbb{E}[r_e(\mathbf{p}(\tau), \tau)]$ is bounded as follows:

$$g_y^2 + \sigma_y^2 \leq \mathbb{E}[r_e(\mathbf{p}(\tau), \tau)] \leq g_y^2 \mathbb{E}[|h(\mathbf{p}_{opt})|^2] + \sigma_y^2. \quad (17)$$

Now, the third term on the RHS of (15) depends on $\mathbf{p}_{opt}$ which further depends on $\mathcal{S}$ in (14). Analytical evaluation of $\mathbb{E}[r_e(\mathbf{p}_{opt}, \tau)]$ is a complicated and non-trivial task that implies calculating $\mathbb{E}[|h(\mathbf{p}_{opt})|^2]$. Nevertheless, by extensive simulations and numerical analysis, we were able to obtain the following analytical approximation:

$$\mathbb{E}[|h(\mathbf{p}_{opt})|^2] \approx a_h \ln\left(\frac{b_h \cdot L}{\lambda} + 1\right) + 1 \quad (18)$$

where a_h and b_h are the shorthand notations for $a_h(\mathbf{p}(k\Delta_s), \Delta_s)$ and $b_h(\mathbf{p}(k\Delta_s), \Delta_s)$, which are two functionals of $\mathbf{p}(k\Delta_s)$ parameterized on Δ_s. For the case in which

$$\mathbf{p}(k\Delta_s) = \begin{bmatrix} \frac{k\Delta_s L}{\alpha T_s} & 0 \end{bmatrix}^T \quad \text{for} \quad k = 0, 1, \cdots, \frac{\alpha T_s}{\Delta_s} \quad (19)$$

we used simulations to evaluate a_h and b_h for different spatial sampling rates[9] given by:

$$S_r = \frac{\alpha T_s \lambda}{\Delta_s L}. \quad (20)$$

To obtain this approximation we first noted that $\mathbb{E}[|h(\mathbf{p}_{opt})|^2]$ depends only on the search space $\mathcal{S}$ and the spatial sampling rate S_r in (20). Since we have selected the search space $\mathcal{S}$ to be a line it is uniquely characterized by its length L. After performing an extensive amount of simulations and plotting the results we noted that for any fixed value of S_r the plot of

[9]The spatial sampling rate is measured as samples per wavelength.

Table I
EVALUATION (BY SIMULATION) OF FUNCTIONALS a_h AND b_h IN (18) FOR DIFFERENT SPATIAL SAMPLING RATES, $S_r = \alpha T_s \lambda / \Delta_s L$

S_r	1	2	4	8	16
a_h	0.9909	1.03	1.061	1.092	1.14
b_h	0.6494	1.057	1.698	1.987	1.907

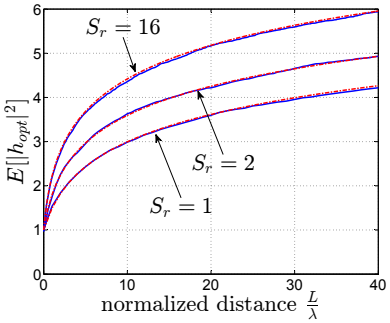

Figure 4. Comparison between the simulated $\mathbb{E}[|h(\mathbf{p}_{opt})|^2]$ (in blue) and its analytical approximation (in red) given by (18) for different spatial sampling rates, S_r.

$\mathbb{E}[|h(\mathbf{p}_{opt})|^2]$ versus L seems to be logarithmic with respect to L. Considering that for $L = 0$ we must have $\mathbb{E}[|h(\mathbf{p}_{opt})|^2] = \mathbb{E}[|h(0)|^2] = 1$ then we proposed the approximation (18) and later we optimized numerically the parameters a_h and b_h for each sampling rate.

The results are summarized in table I. In addition, as illustrated by Fig. 4, the proposed analytical approximation in (18) is virtually indistinguishable from the actual mean $\mathbb{E}[|h(\mathbf{p}_{opt})|^2]$, this shows the validity of our approximations. Note that in (19) the number $\frac{\alpha T_s}{\Delta_s}$ must be an integer, and so we can write:

$$\Delta_s = \frac{\alpha T_s}{N} \quad (21)$$

where N a positive integer.

Now consider the fourth and fifth terms on the RHS of (15). We need a control law that takes the robot from its initial position along a straight line of length L, stops the robot at the end of that line and finally make it move to $\mathbf{p}_{opt}$. In addition, this must be done using the minimum amount of mechanical energy. Using the result in the Appendix it is not difficult to show that this optimal control law for phase 1 is given by:

$$\begin{aligned} \mathbf{u}_1^*(t) &= L \cdot [1\ 1]^T \\ &\cdot \left(K_{u1}(\alpha T_s) e^{\frac{-t}{\sqrt{\tau_v}}} + K_{u2}(\alpha T_s) e^{\frac{t}{\sqrt{\tau_v}}} + K_{u3}(\alpha T_s)\right), \\ &\text{where } t \in [0, \alpha T_s] \end{aligned} \quad (22)$$

with τ_v the constant time for the translational motion which is a function of the system's parameters (see Appendix for

details). Similarly, for the phase 2 is:

$$\begin{aligned}\mathbf{u}_2^*(t) &= \|[L\ 0]^T - \mathbf{q}_{opt}\|_2 \cdot [1\ 1]^T \\ &\cdot \left(K_{u1}((1-\alpha)T_s) e^{\frac{-(t-\alpha T_s)}{\sqrt{\tau_v}}} + K_{u2}((1-\alpha)T_s) e^{\frac{t-\alpha T_s}{\sqrt{\tau_v}}} \right. \\ &+ \left. K_{u3}((1-\alpha)T_s) \right), \\ &\text{where } t \in (\alpha T_s, T_s].\end{aligned} \tag{23}$$

Using these optimal control laws and by performing some cumbersome algebra on (1) and (4), we can show that the mechanical energy consumed during phase 1 is:

$$E_{mech}(\mathbf{u}_1(t), 0, \alpha T_s) = m_2(\alpha T_s) L^2 \tag{24}$$

and the mechanical energy consumed during phase 2 is:

$$E_{mech}(\mathbf{u}_2(t), \alpha T_s, T_s) = m_2((1-\alpha)T_s) \|[L\ 0]^T - \mathbf{q}_{opt}\|_2^2 \tag{25}$$

where $m_2(t)$ is given by (26) with $K_{v1}(t_0)$, $K_{v2}(t_0)$ and $K_{v3}(t_0)$ defined in (53). Now, using the proposed approximation (18), and substituting (16), (24) and (25) into (15) we obtain

$$\begin{aligned}\mathbb{E}[E_s(0,T)] &\approx \eta \alpha T_s \left(g_y^2 + \sigma_y^2 \right) \\ &+ \eta \int_{\alpha T_s}^{T_s} \mathbb{E}[r_e(\mathbf{p}(\tau), \tau)] d\tau \\ &+ \eta (T - T_s) g_y^2 \left(a_h \ln \left(\frac{b_h \cdot L}{\lambda} + 1 \right) + 1 \right) \\ &+ \eta (T - T_s) \sigma_y^2 - m_2(\alpha T_s) L^2 \\ &- m_2((1-\alpha)T_s) \mathbb{E}[\|[L\ 0]^T - \mathbf{q}_{opt}\|_2^2].\end{aligned} \tag{27}$$

For the case where $S_r \to \infty$ in (20) (according to experimental results $S_r \geq 8Sa/\lambda$ will perform similarly to $S_r \to \infty$) we have that $\|[L\ 0]^T - \mathbf{q}_{opt}\|_2$ becomes a continuous random variable uniformly distributed between 0 and L. Thus, $\mathbb{E}[\|[L\ 0]^T - \mathbf{q}_{opt}\|_2^2] = \frac{L^2}{3}$ and if we consider the inequality (17) then after doing simple algebra we obtain both a lower bound:

$$\begin{aligned}\mathbb{E}[E_s(0,T)] &> \eta T \left(g_y^2 + \sigma_y^2 \right) \\ &+ \eta (T - T_s) g_y^2 a_h \ln \left(\frac{b_h \cdot L}{\lambda} + 1 \right) \\ &- \left(m_2(\alpha T_s) + \frac{1}{3} m_2((1-\alpha)T_s) \right) \cdot L^2 \\ &= f_L(L, \alpha, T_s),\end{aligned} \tag{28}$$

and an upper bound:

$$\begin{aligned}\mathbb{E}[E_s(0,T)] &< \eta T \left(g_y^2 + \sigma_y^2 \right) \\ &+ \eta (T - \alpha T_s) g_y^2 a_h \ln \left(\frac{b_h \cdot L}{\lambda} + 1 \right) \\ &- \left(m_2(\alpha T_s) + \frac{1}{3} m_2((1-\alpha)T_s) \right) \cdot L^2 \\ &= f_U(L, \alpha, T_s).\end{aligned} \tag{29}$$

Therefore instead of maximizing $\mathbb{E}[E_s(0,T)]$, for which we do not have an analytical expression, we can optimize its bounds, i.e., either $f_L(L, \alpha, T_s)$ or $f_U(L, \alpha, T_s)$. If we optimize the upper bound $f_U(L, \alpha, T_s)$ we risk obtaining a behaviour in which the average of the energy harvested is lower than the average energy used for the motion, because the energy harvested is over-estimated in this bound. On the other hand if we optimize the lower bound $f_L(L, \alpha, T_s)$ then we eliminate this risk because the energy harvested is under-estimated in this other bound. Therefore we will proceed to maximize the lower bound $f_L(L, \alpha, T_s)$.

Now, we can maximise $f_L(L, \alpha, T_s)$ by simultaneously solving the following set of equations:

$$\begin{aligned}\tfrac{\partial f_L(L,\alpha,T_s)}{\partial L} &= 0, \\ \tfrac{\partial f_L(L,\alpha,T_s)}{\partial \alpha} &= 0, \\ \tfrac{\partial f_L(L,\alpha,T_s)}{\partial T_s} &= 0.\end{aligned} \tag{30}$$

Solving for the optimal length L the first equation in (30) gives:

$$\begin{aligned}L_{opt}(\alpha, T_s) &= \frac{1}{2} \sqrt{\frac{\lambda^2}{b_h^2} + \frac{2\eta(T - T_s) g_y^2 a_h}{m_2(\alpha T_s) + \frac{1}{3} m_2((1-\alpha)T_s)}} \\ &- \frac{\lambda}{2 b_h}.\end{aligned} \tag{31}$$

The objective of this technique is to obtain gain from the small-scale fading which varies considerably over small distances. In practice if L is too big then the shadowing and the path-loss effects cannot be considered constant anymore (as we have assumed at the beginning of this article) and consequently this technique may not work properly anymore. Therefore in order to avoid this problem we will limit the maximum value of L to some predefined value L_{max} and so the bounded optimal value for L is:

$$L_{opt}^b(\alpha, T_s) = \begin{cases} L_{opt}(\alpha, T_s), & \forall\ L_{opt}(\alpha, T_s) < L_{max} \\ L_{max}, & \text{otherwise.} \end{cases} \tag{32}$$

Since the shadowing can usually be considered constant for distances of a few wavelengths then we would suggest selecting $L_{max} < 10\lambda$.

Now, if we substitute for L in $f_L(L, \alpha, T_s)$ with (32) then we obtain the modified cost function $f_m(\alpha, T_s)$. We have to note that since $\alpha \in (0, 1)$ and $T_s \in (0, T)$ the domain of $f_m(\alpha, T_s)$ is finite. If we discretize this domain by applying a fine enough grid and then we use simulated annealing [33] to maximize $f_m(\alpha, T_s)$ over this grid we can ensure that we obtain a solution sufficiently close to the global maximum.

So now we have completed the optimization of the MR-EHT (i.e., we have shown how to maximize the net average stored energy, $\mathbb{E}[E_s(0,T)]$). In the next section we will look at the estimator for $\mathbf{p}_{opt}$.

V. Estimation of Optimal Location ($\mathbf{p}_{opt}$)

In this section, we illustrate how the optimal location $\mathbf{p}_{opt}$ can be estimated from the noisy signal $r_e(k)$ in (8) (shorthand for $r_e(\mathbf{p}(k\Delta_s), k\Delta_s)$). This process is done once the robot

$$
\begin{aligned}
m_2(t_0) &= 2\Bigg[\left(\frac{\sqrt{\tau_v}K_{u1}(t_0)}{2}\right)\cdot\left(c_1K_{u1}(t_0)-\frac{c_2}{r}K_{v1}(t_0)\right)\cdot\left(1-e^{\frac{-2t_0}{\sqrt{\tau_v}}}\right)\\
&+ \sqrt{\tau_v}\left(2c_1K_{u1}(t_0)K_{u3}(t_0)-\frac{c_2}{r}\left(K_{u1}(t_0)K_{v3}(t_0)+K_{v1}(t_0)K_{u3}(t_0)\right)\right)\cdot\left(1-e^{\frac{-t_0}{\sqrt{\tau_v}}}\right)\\
&+ \left(c_1(2K_{u1}(t_0)K_{u2}(t_0)+K_{u3}^2(t_0))-\frac{c_2}{r}(K_{u1}(t_0)K_{v2}(t_0)+K_{v1}(t_0)K_{u2}(t_0)+K_{u3}(t_0)K_{v3}(t_0))\right)t_0\\
&+ \sqrt{\tau_v}\left(2c_1K_{u2}(t_0)K_{u3}(t_0)-\frac{c_2}{r}(K_{u2}(t_0)K_{v3}(t_0)+K_{v2}(t_0)K_{u3}(t_0))\right)\cdot\left(e^{\frac{t_0}{\sqrt{\tau_v}}}-1\right)\\
&+ \left(\frac{\sqrt{\tau_v}K_{u2}(t_0)}{2}\right)\cdot\left(c_1K_{u2}(t_0)-\frac{c_2}{r}K_{v2}(t_0)\right)\cdot\left(e^{\frac{2t_0}{\sqrt{\tau_v}}}-1\right)\Bigg] \qquad (26)
\end{aligned}
$$

finishes the phase 1 of the dead time. Let the sampling period be $\Delta_s = \frac{\alpha T_s}{N}$ and so the robot will use $N+1$ measurements $[r_e(0),\ r_e(1),\ldots,r_e(N)]$. The MR can use a linear smoother to reduce the effect of the post-rectifier noise $n_r(t)$ in (8). Then it can employ the output of the smoother $r_s(k)$ instead of the signal $r_e(k)$ to obtain a better estimate for $\mathbf{p}_{opt}$. So, the estimation of $\mathbf{p}_{opt}$ can be performed as follows:

$$\hat{\mathbf{p}}_{opt} = \mathbf{p}(k_{opt}), \qquad (33)$$

where

$$k_{opt} = \arg\max_k r_s(k), \qquad (34)$$

and

$$r_s(k) = \sum_{m=0}^{N} \beta_{k,m}^* r_e(m). \qquad (35)$$

Now, the optimal weights ($\beta_{k,m}^*$) for the linear smoother are calculated as follows:

$$\boldsymbol{\beta}_k^* = \arg\min_{\boldsymbol{\beta}_k} J(\boldsymbol{\beta}_k) \qquad (36)$$

with

$$J(\boldsymbol{\beta}_k) = \mathbb{E}\left[\left(r_s(k) - g_y^2|h(\mathbf{p}(k))|^2\right)^2\right] \qquad (37)$$

where $\boldsymbol{\beta}_k = [\beta_{k,0},\ \beta_{k,1},\ \ldots,\beta_{k,N}]^T$ and

$$
\begin{aligned}
J(\boldsymbol{\beta}_k) &= \mathbb{E}\left[r_s^2(k) - 2g_y^2 r_s(k)|h(\mathbf{p}(k))|^2 + g_y^4|h(\mathbf{p}(k))|^4\right]\\
&= \mathbb{E}\left[\left(\sum_{m=0}^{N}\beta_{k,m}r_e(m)\right)^2\right]\\
&- 2g_y^2\sum_{m=0}^{N}\beta_{k,m}\mathbb{E}\left[r_e(m)|h(\mathbf{p}(k))|^2\right]\\
&+ g_y^4\mathbb{E}\left[|h(\mathbf{p}(k))|^4\right]. \qquad (38)
\end{aligned}
$$

So setting

$$\nabla_{\boldsymbol{\beta}_k} J(\boldsymbol{\beta}_k) = \mathbf{0}, \qquad (39)$$

where $\nabla_{\boldsymbol{\beta}_k} = [\frac{\partial}{\partial\beta_{k,0}},\ \frac{\partial}{\partial\beta_{k,1}},\ldots,\ \frac{\partial}{\partial\beta_{k,N}}]^T$ and

$$
\begin{aligned}
\frac{\partial J(\boldsymbol{\beta}_k)}{\partial\beta_{k,i}} &= 2\sum_{m=0}^{N}\beta_{k,m}\mathbb{E}\left[r_e(m)r_e(i)\right]\\
&- 2g_y^2\mathbb{E}\left[r_e(i)|h(\mathbf{p}(k))|^2\right] \qquad (40)
\end{aligned}
$$

then it is not difficult to show that:

$$
\begin{aligned}
\mathbb{E}\left[r_e(i)|h(\mathbf{p}(k))|^2\right] &= g_y^2\mathbb{E}\left[|h(\mathbf{p}(i))|^2|h(\mathbf{p}(k))|^2\right] + \sigma_y^2\\
&= g_y^2 J_0^2\left(\frac{2\pi\|\mathbf{p}(i)-\mathbf{p}(k)\|_2}{\lambda}\right) + g_y^2\\
&+ \sigma_y^2 \qquad (41)
\end{aligned}
$$

$$
\begin{aligned}
\mathbb{E}\left[r_e(i)r_e(m)\right] &= g_y^4\left(J_0^2\left(\frac{2\pi\|\mathbf{p}(i)-\mathbf{p}(m)\|_2}{\lambda}\right)+1\right)\\
&+ 2g_y^2\sigma_y^2 + \sigma_y^4 + \sigma_r^2,\ i\neq m \qquad (42)
\end{aligned}
$$

and

$$\mathbb{E}\left[r_e^2(i)\right] = 2g_y^4 + 8g_y^2\sigma_y^2 + 8\sigma_y^4 + \sigma_r^2,\ i = m. \qquad (43)$$

Therefore, if we know σ_y^2, σ_r^2 and g_y^2 (or we can estimate them) then we can evaluate (41), (42) and (43) and use in (40) to calculate an analytical expression for the gradient $\nabla_{\boldsymbol{\beta}_k} J(\boldsymbol{\beta}_k)$. So, we can solve (39) and obtain the optimal weights for the smoother in (35) in order to estimate $\mathbf{p}_{opt}$ with (33).

VI. Simulation and Results

With the analytical framework developed in the previous sections, our objective now is to provide further insights by employing extensive simulations. To this end, we divide this section into two parts. In the first part, we analyze the MR-EHT approach in a noiseless scenario assuming that $\hat{\mathbf{p}}_{opt} = \mathbf{p}_{opt}$, (i.e., that $\mathbf{p}_{opt}$ is exactly known by the MR). Then, in the second part we consider a noisy scenario and we analyze how the estimation error in $\hat{\mathbf{p}}_{opt}$ affects the energy harvested during the resting time in phase 3. We also observe how the optimal smoother described in section V can mitigate the degradation in the stored energy due to estimation error in the optimal resting position.

We will take the parameter values of [27] for the DDR since these values were obtained experimentally and therefore represent a real robot. This will allow us to get more realistic results in our simulations. In table II we show the MR's parameters. In addition, since the performance of the system depends on ηg_y^2 and $\eta\sigma_y^2$ and not on individual values of η we can assume for simulation purposes, without any loss of generality, $\eta = 1$ in (10).

Table II
MOBILE ROBOT PARAMETERS

$c_1 = 202.8169$W	$c_2 = 14.8885$N	$r = 9.5$cm
$c_A = 1.1279$Nm	$c_B = 14.8885$Nm	$b = 16.5$cm
$J_1 = 7 \cdot 10^{-2}$	$J_2 = 1.3 \cdot 10^{-3}$	

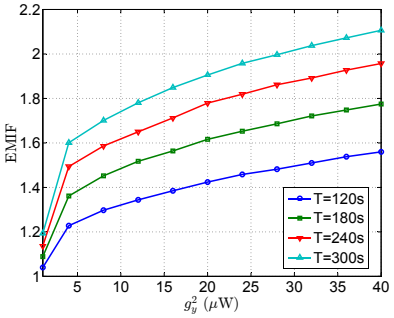

Figure 5. Comparison of EMIF vs g_y^2 (i.e., average received power) for different dead times T, with $N = \lceil \frac{16L_{opt}}{\lambda} \rceil$ and $\lambda = 6$cm (which corresponds to a carrier frequency of 5GHz).

A. Energy Harvesting Performance without Noise

Although ignoring the noise for the proposed technique would seem unrealistic, it is of practical interest to analyze the behaviour of the MR-EHT under such a consideration since it represents an upper bound on the performance of the proposed algorithm and also describes the behaviour of our technique when $SNR = \frac{g_y^2}{\sigma_y^2+\sigma_r^2}$ is high.

In order to evaluate the performance of the harvesting technique, we now define a new metric called the "Energy Mobility Improvement Factor" (EMIF):

$$EMIF = \frac{\mathbb{E}[E_s(0,T)]}{\eta g_y^2 T}. \tag{44}$$

The numerator in (44) corresponds to the average net energy stored during the total dead time T while using mobility to harvest energy. The denominator is the expected value of the energy that the robot would harvest if it did not move at all. This metric quantifies how much the average net stored energy has been increased by moving the robot in comparison to the case where the robot does not move at all, and so we want $EMIF > 1$.

We consider first the case in which the signal transmitted by the BS uses a carrier frequency of 5GHz (corresponding to a wavelength of 6cm). In Figs. 5 and 6 we can see the performance of the MR-EHT for a spatial sampling rate[10] $S_r > 16Sa/\lambda$, different dead times T and different average powers received g_y^2.

From these Figs. we first observe that indeed $EMIF > 1$ which shows that the optimal energy harvesting approach is to use intelligent motion. We also observe that EMIF is a nonlinear increasing function of both the dead time T and g_y^2, and so the higher the dead time T and/or the higher is g_y^2 then the larger will be the EMIF. In other words, when

[10]This is obtained by making $N = \lceil \frac{16L_{opt}}{\lambda} \rceil$ in (21) with L_{opt} the optimal line length.

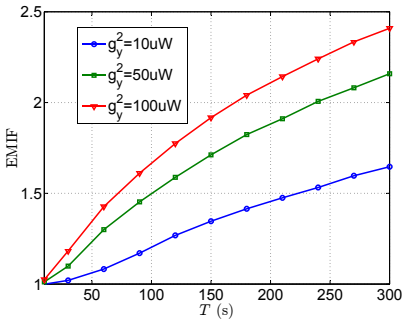

Figure 6. Comparison of EMIF vs T for different average received powers g_y^2, with $N = \lceil \frac{16L_{opt}}{\lambda} \rceil$ and $\lambda = 6$cm (which corresponds to a carrier frequency of 5GHz).

the dead time and/or the average received power are above a certain minimum our technique is more beneficial. Now, it is interesting to observe in Fig. 5 that if the robot has a dead time T of just 2 minutes and receives an average power $g_y^2 = 40\mu W$ then $EMIF > 1.5$, which implies that by optimally moving the robot the stored energy has increased by more than 50%. In a more beneficial case, for example with a dead time of $T = 5$min and an average receiving power of $g_y^2 = 50\mu W$, the benefit of moving the robot is even greater producing an EMIF higher than 2, i.e., an increase of more than 100% (see Fig. 6).

Now, in order to observe the effect of the wavelength of the RF signal transmitted by the BS we repeated exactly the same simulations but changed the wavelength to 14.02cm (which corresponds to a carrier frequency of 2.14GHz). So comparing Figs. 5 and 6 with 7 and 8 we observe that EMIF is considerably lower for the carrier frequency of 2.14GHz than for 5GHz.

This can be explained as follows: consider two robots using the same EHT described in this article. Let the first robot receive a signal with wavelength λ_1 and let the second robot receive a signal of wavelength $\lambda_2 > \lambda_1$. If both robots move just one wavelength then the energy harvested will be the same since this energy depends only on the normalized distance (see (18)) but the second robot will have to travel a longer distance than the first one and so it will use a greater amount of mechanical energy. Thus the net energy stored (see (9)) by the second robot will be lower. This means that given the same conditions of received power and dead time duration our harvesting technique works better for small wavelengths. Nevertheless we should remark that the path loss increases with frequency [34]. Thus in the system using a smaller wavelength either the MR would have to be closer to the BS or the BS would have to transmit with higher power to meet the same conditions of received power as the system using a higher wavelength.

In Fig. 9, we observe the behaviour of $\mathbb{E}[|h_{\mathbf{opt}}|^2]$ as a function of the sampling rate S_r. We can observe it tends to saturate for a certain value of S_r and then in the noiseless case there is no reason to select S_r greater than $\approx 8Sa/\lambda$. But, as we shall see in the next subsection, higher values of S_r help to better estimate $\mathbf{p}_{opt}$ when noise is present.

As we mentioned earlier in this paper the optimization of

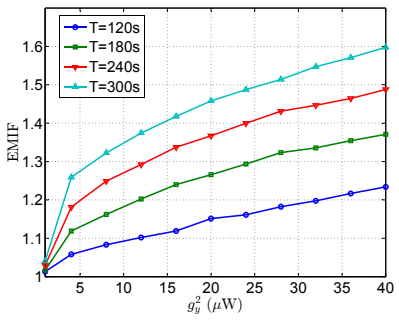

Figure 7. Comparison of EMIF vs g_y^2 (i.e., average received power) for different dead times T, with $N = \lceil \frac{16L_{opt}}{\lambda} \rceil$ and $\lambda = 14.02$cm (which corresponds to a carrier frequency of 2.14GHz).

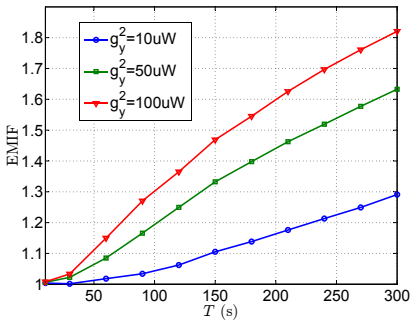

Figure 8. Comparison of EMIF vs T for different average received powers g_y^2, with $N = \lceil \frac{16L_{opt}}{\lambda} \rceil$ and $\lambda = 14.02$cm (which corresponds to a carrier frequency of 2.14GHz).

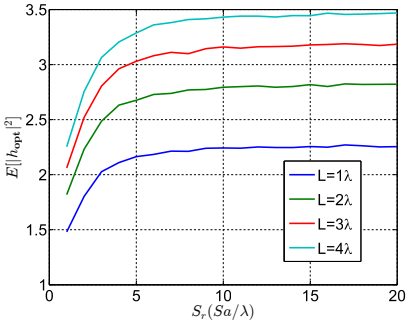

Figure 9. Behaviour of $\mathbb{E}[|h_{\mathbf{opt}}|^2]$ as a function of the spatial sampling rate S_r parameterized on different lengths of the exploration line (L).

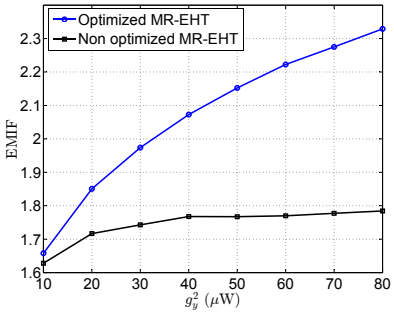

Figure 10. Comparison of the EMIF vs g_y^2 (i.e., average received power) for the optimized MR-EHT and a non-optimized MR-EHT both with a dead time $T = 300$s, $N = \lceil \frac{16L_{opt}}{\lambda} \rceil$ and $\lambda = 6$cm (which corresponds to a carrier frequency of 5GHz).

the parameters is very important. To illustrate, in figure 10 we plot EMIF as a function of the average received power with a dead time of $T = 300$s for two cases: (i) in the first case, we implement the MR-EHT with optimized parameters (see section IV); (ii) in the second case, we implement the MR-EHT without the optimized parameters and we arbitrarily select for this case $\alpha = 0.5$, $T_s = 100$s and $L = 0.8\lambda$. As we can see in figure 10 the non-optimized version has in some cases a much lower performance (as expected) than the optimized case. This illustrates the importance of implementing the MR-EHT with the optimized parameters.

We illustrate the behaviour of the optimal values of L, α and T_s in the figures 11 and 12. It is worth noticing that although L_{opt} is an increasing function of g_y^2 and T, we observe that $T_{s_{opt}}$ is an increasing function of g_y^2 but a decreasing function of T. This behaviour of T_s means that for a fixed received power g_y^2, if we increase the dead time T the robot will complete phases 1 and 2 slower to save more mechanical energy and increase the net stored energy. On the other hand if the dead time T is fixed but we increase the received power g_y^2 then the robot will complete phases 1 and 2 faster to increase the duration of the resting time (phase 3). By doing so the robot increases the amount of energy harvested during this last phase and thus increases the net stored energy. Finally, it is also interesting to note that α_{opt} is independent of g_y^2 and is almost constant[11] for $T > 60$secs.

As mentioned earlier in this article the channel coherence time is considered longer than the dead time (see definition in the Introduction and at the start of section III). So according to the values T presented in this simulation section it would seem that we are considering unrealistic values since in mobile communications coherence times are at most on the order of a couple of seconds or even miliseconds. Nevertheless, as mentioned earlier in the article, we are considering that the MR works in a extremely low mobility environment. Now, in [35] a narrow band wireless channel operating at a 2.4GHz in an environment with very little movement was experimentally characterized and the coherence time (referred to as time duration for which the temporal autocorrelation is higher than 90% of its maximum value) is 50 seconds. Therefore it seems natural that environments with extremely low mobility like museums at night or caves without people can exhibit coherence times on the order of a couple of minutes or at least tens of seconds.

B. Energy Harvesting Performance with Noise

In this section, we consider the effect of the noise on the estimation of $\mathbf{p_{opt}}$ and its effect on the harvested energy (10) during the resting time (i.e., $t \in [T_s, T]$). Define $P_n = \sigma_y^2 + \sigma_r^2$ as the total noise power, i.e., the power of the pre-rectifier

[11]The optimal value of α was derived by optimizing $f_T(L, \alpha, T_s)$ which is a valid approximation for $\mathbb{E}[E_s(0,T)]$ as long as $S_r \geq 8Sa\lambda$. Therefore for values $S_r < 8Sa\lambda$ this behaviour may change slightly.

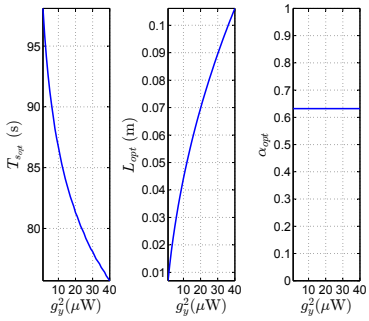

Figure 11. Optimal parameter values of $f_L(L, \alpha, T_s)$ vs g_y^2 for $T = 300$s, with $\lambda = 14.02$cm (which corresponds to a carrier frequency of 2.14GHz).

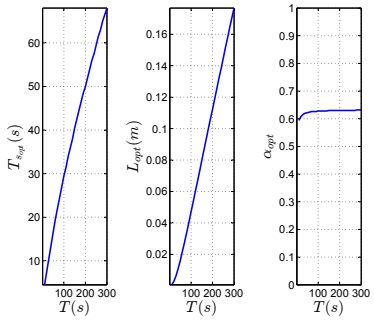

Figure 12. Optimal parameter values of $f_L(L, \alpha, T_s)$ vs T for $g_y^2 = 100\mu$W, with $\lambda = 14.02$cm (which corresponds to a carrier frequency of 2.14GHz).

noise plus the power of the post-rectifier noise . Also let $\sigma_y^2 = \alpha_n P_n$ and $\sigma_r^2 = (1-\alpha_n)P_n$ with $\alpha_n \in (0,1)$. Finally define the SNR as $10\log_{10}\left(\frac{g_y^2}{P_n}\right)$. Let us consider three cases: (i) in the first case we consider that $\mathbf{p}_{opt}$ is estimated as in (33) using the optimal smoother of section V and we will denote this estimate by $\hat{\mathbf{p}}_{opt}^{'}$; (ii) in the second case we consider that $\mathbf{p}_{opt}$ is estimated as in (33) but using the signal $r_e(k)$ instead of $r_s(k)$, the output of the smoother (35). We will denote this estimate by $\hat{\mathbf{p}}_{opt}^{''}$; (iii) in the last case assume that the robot knows exactly $\mathbf{p}_{opt}$. While this case is unrealistic it will serve us for comparison.

We consider two scenarios with a low SNR of 0dB, line length $L = 1\lambda$, different values of α_n (for $\sigma_y^2 = \alpha_n P_n$ and for $\sigma_r^2 = (1-\alpha_n)P_n$) and two values of the spatial sampling rate: $S_r = 16Sa/\lambda$ and $S_r = 8Sa/\lambda$. In table III we observe the degradation[12] of the energy harvested during the third phase. In the first row we observe the degradation suffered when the MR uses the estimate $\hat{\mathbf{p}}_{opt}^{'}$ and in the second row we observe the degradation when the MR uses the estimate $\hat{\mathbf{p}}_{opt}^{''}$ mentioned above.

From tables III and IV we see that the harvested energy degradation is lower for higher values of the spatial sampling rate S_r. This means that while in the noiseless scenario there is no reason to select a value of $S_r > 8Sa/\lambda$, in the noisy scenario taking higher values of S_r helps to combat the degradation of the energy harvested.

[12]The degradation is mathematically expressed as the ratio of the energy harvested during the resting time when $\hat{\mathbf{p}}_{opt} \neq \mathbf{p}_{opt}$ over the energy harvested during the resting time when $\hat{\mathbf{p}}_{opt} = \mathbf{p}_{opt}$. This ratio shows us how much the energy harvested has decreased due to the estimation error in $\hat{\mathbf{p}}_{opt}$.

Table III
HARVESTED ENERGY DEGRADATION FOR $S_r = 16Sa/\lambda$

α_n	0.3	0.5	0.9
$\frac{\mathbb{E}[E_r(\hat{\mathbf{p}}_{opt}^{'},T_s,T)]}{\mathbb{E}[E_r(\mathbf{p}_{opt},T_s,T)]}$	0.8731	0.8761	0.9004
$\frac{\mathbb{E}[E_r(\hat{\mathbf{p}}_{opt}^{''},T_s,T)]}{\mathbb{E}[E_r(\mathbf{p}_{opt},T_s,T)]}$	0.8209	0.8070	0.8315

Table IV
HARVESTED ENERGY DEGRADATION FOR $S_r = 8Sa/\lambda$

α_n	0.3	0.5	0.9
$\frac{\mathbb{E}[E_r(\hat{\mathbf{p}}_{opt}^{'},T_s,T)]}{\mathbb{E}[E_r(\mathbf{p}_{opt},T_s,T)]}$	0.8296	0.8449	0.8580
$\frac{\mathbb{E}[E_r(\hat{\mathbf{p}}_{opt}^{''},T_s,T)]}{\mathbb{E}[E_r(\mathbf{p}_{opt},T_s,T)]}$	0.8018	0.8139	0.8222

It is also interesting that the degradation of the energy harvested is not only a function of the SNR but also a function of α_n, (i.e., depending on the individual powers of the pre-rectifier noise $\sigma_y^2 = \alpha_n P_n$ and the power of the post-rectifier noise $\sigma_r^2 = (1-\alpha_n)P_n$). The degradation is higher for low values of α_n (see tables III and IV) which implies that the post-rectifier noise is more harmful to our technique than the pre-rectifier noise. Therefore, the RF designers should pay more attention to reducing the post-rectifier noise than the pre-rectifier noise when designing the energy harvesting receiver of figure 2.

Finally, note that the ranges of received power considered for the simulations are actually achievable in practice. To confirm this first note that in [36] the authors used a transmitter with an RF carrier frequency of 2388 MHz (close to the frequencies considered in this article) that generated a power density of $170\mathrm{mW/cm}^2$ at a distance of 1.54km. This was achieved using a directional antenna with a large parabolic reflector (26m radius) and high transmission power (450 kW). Therefore it is indeed possible in practice to achieve received powers on the order of tens of microwats (as used in simulations) at distances of the order the tens or hundreds of meters using significantly lower transmission power and a significantly smaller parabolic reflector for the antenna.

VII. CONCLUSIONS

We have shown that when harvesting radio energy with a MR the average, net amount of energy stored (i.e., the average energy harvested minus the average energy used for movement) is higher when the robot is moved in an optimal way than when the robot simply stands still. This implies that the optimal behaviour for a MR using wireless energy harvesting under a flat-fading wireless channel is to move in an optimal way instead of not moving. We also showed how to derive this optimal movement as a function of the dead time duration and the wireless power received. So while we have shown (for the first time) that intelligent mobility based energy harvesting increases efficiency, future work will examine how we can optimize the MR's trajectory (i.e., as opposed to restricting it to a straight line). We will also devise

an improved intelligent control (i.e., $\mathbf{u}(t)$ in (1)) in order to perform a more efficient search over the trajectory.

APPENDIX
OPTIMAL CONTROL LAW FOR DDR

In this Appendix, we obtain the optimal control law so that the DDR described by equations (1)-(4) uses minimum energy to do the following: (i) starting with the still (i.e., $v(0) = 0$ at the initial position $\mathbf{p}(0)$, (ii) moving in a straight line of length l, (iii) stopping at the end of the straight line (i.e., $v(t_f) = 0$). Mathematically this optimization problem (OP) consists in optimizing the functional $E_{mech}(\mathbf{u}(t), 0, t_f)$ subject to some restrictions:

$$\underline{\mathbf{OP}}: \quad \min_{u_R(t)} \int_0^{t_f} \left(c_1 \mathbf{u}^T(t)\mathbf{u}(t) - c_2[v(t) \;\; 0]\mathbf{T}_{\mathbf{q}}^{-T}\mathbf{u}(t)\right)dt \tag{45}$$

s.t.

$$\dot{v}(t) + [1 \;\; 0]\bar{\mathbf{A}}[v(t) \;\; 0]^T = [1 \;\; 0]\bar{\mathbf{B}}\mathbf{u}(t), \tag{46}$$

$$\int_0^{t_f} v(t)dt = l, \tag{47}$$

$$u_R(t) = u_L(t) \tag{48}$$

$$v(0) = 0, \qquad v(t_f) = 0. \tag{49}$$

The differential constraint (46) corresponds to the state equation that describes how the velocity $v(t)$ is controlled by the control input $\mathbf{u}(t)$. We must also satisfy the isoperimetric [37] constraint (47) that makes the robot advance a distance l, and satisfy the boundary conditions (49) which estate that the robot starts from rest and finishes at rest. Finally, we must satisfy the constraint (48) to ensure that the robot moves in straight.

The optimization problem **OP** is a classical problem of optimum control and can be solved using calculus of variations [37], [38]. By applying this method we arrive at the following second order differential equation:

$$\ddot{v}(t) - [1 \;\; 0]\left(\mathbf{Q}^T\mathbf{Q}[v(t) \;\; 0]^T + \bar{\mathbf{B}}\bar{\mathbf{B}}^T\begin{bmatrix}\frac{\alpha}{2c_1} & 0\end{bmatrix}^T\right) = 0 \tag{50}$$

where α is the Lagrange multiplier for constraint (47) and

$$\mathbf{Q}^T\mathbf{Q} = \bar{\mathbf{A}}^T\bar{\mathbf{A}} - \left(\frac{c_2}{c_1}\right)\bar{\mathbf{B}}\bar{\mathbf{B}}^T\mathbf{T}_{\mathbf{q}}^{-T}\bar{\mathbf{B}}^{-1}\bar{\mathbf{A}}. \tag{51}$$

By solving (50) and satisfying the conditions (49) we get:

$$v(t) = \left(K_{v1}(t_f)e^{\frac{-t}{\sqrt{\tau_v}}} + K_{v2}(t_f)e^{\frac{t}{\sqrt{\tau_v}}} + K_{v3}(t_f)\right)\cdot l \tag{52}$$

where $\tau_v = \frac{c_A(k_1c_A - k_2c_B)}{k_1(J_1+J_2)^2}$ and:

$$\begin{aligned}
K_{v1}(t_f) &= \frac{1-e^{\frac{t_f}{\sqrt{\tau_v}}}}{4\sqrt{\tau_v}\left(1-\cosh\left(\frac{t_f}{\sqrt{\tau_v}}\right)\right)+2t_f\sinh\left(\frac{t_f}{\sqrt{\tau_v}}\right)},\\
K_{v2}(t_f) &= \frac{e^{\frac{-t_f}{\sqrt{\tau_v}}}-1}{4\sqrt{\tau_v}\left(1-\cosh\left(\frac{t_f}{\sqrt{\tau_v}}\right)\right)+2t_f\sinh\left(\frac{t_f}{\sqrt{\tau_v}}\right)},\\
K_{v3}(t_f) &= \frac{2\sinh\left(\frac{t_f}{\sqrt{\tau_v}}\right)}{4\sqrt{\tau_v}\left(1-\cosh\left(\frac{t_f}{\sqrt{\tau_v}}\right)\right)+2t_f\sinh\left(\frac{t_f}{\sqrt{\tau_v}}\right)}.
\end{aligned} \tag{53}$$

Finally, using (52) with (48) and (46) we obtain the optimal control law:

$$\mathbf{u}^*(t) = \begin{bmatrix} K_{u1}(t_f)e^{\frac{-t}{\sqrt{\tau_v}}} + K_{u2}(t_f)e^{\frac{t}{\sqrt{\tau_v}}} + K_{u3}(t_f) \\ K_{u1}(t_f)e^{\frac{-t}{\sqrt{\tau_v}}} + K_{u2}(t_f)e^{\frac{t}{\sqrt{\tau_v}}} + K_{u3}(t_f) \end{bmatrix}\cdot l \tag{54}$$

where:

$$\begin{aligned}
K_{u1}(t_f) &= \left(\frac{c_A - \frac{J_1+J_2}{\sqrt{\tau_v}}}{c_B r}\right)K_{v1}(t_f),\\
K_{u2}(t_f) &= \left(\frac{c_A + \frac{J_1+J_2}{\sqrt{\tau_v}}}{c_B r}\right)K_{v2}(t_f),\\
K_{u3}(t_f) &= \left(\frac{c_A}{c_B r}\right)K_{v3}(t_f).
\end{aligned} \tag{55}$$

REFERENCES

[1] M. Grosslauser and D.N.Tse, "Mobility increases the capacity of ad hoc wireless networks," *IEEE/ACM Transactions on Networking*, vol. 10, no. 4, 2002.

[2] D. Bonilla, D. McLernon, M. Ghogho, and S. A. R. Zaidi, "An energy saving robot mobility diversity algorithm for wireless communications," *Proceedings of the 21st European Signal Processing Conference (EUSIPCO)*, September 2013.

[3] D. Bonilla, D. McLernon, and M. Ghogho, "A robotic mobility diversity algorithm with markovian trajectory planners," *Proceedigns of the 23rd IEEE International Workshop on Machine Learning for Signal Processing (MLSP)*, September 2013.

[4] R. Murai, T. Sakai, H. Kawano, and Y. Matsukawa, "A novel visible light communication system for enhanced control of autonomous delivery robots in a hospital," *Proceedigns of International Symposium on System Integration (SII)*, 2012.

[5] J. M. Smith, M. P. Oliveri, A. Lackpour, and N. Hinnerschitz, "Search and rescue robots: the civil protection teams of the future," *Proc. of Third International Conference on Emerging Security Technologies (EST)*, 2012.

[6] B. Mobedi and G. Nejat, "3-d active sensing in time-critical urban search and rescue missions," *IEEE/ASME Transactions on Mechatronics*, vol. 17, no. 6, December 2012.

[7] J. K. S.L.S. Robin R. Murphy and R. Shoureshi, "Mobility robots in mine rescue and recovery," *IEEE Robotics & Automation Magazine*, vol. 16, no. 2, 2009.

[8] S. kook Yun and D. Rus, "Adaptive coordinating construction of truss structures using distributed equal-mass partitioning," *IEEE Transactions on robotics*, vol. 30, no. 1, February 2014.

[9] J.-H. Kim, G. Sharma, and S. S. Iyengar, "Famper: A fully autonomous mobile robot for pipeline exploration," *Proceedigns of the IEEE International Conference on Industrial Technology (ICIT)*, 2010.

[10] H.-T. Lee, W.-C. Lin, C.-H. Huang, and Y.-J. Huang, "Wireless indoor surveillance robot," *Proceedigns of SICE annual conference*, 2011.

[11] N. Suzuki and Y. Yamamoto, "Pursuing entertainment aspects of sony aibo quadruped robots," *Proceedigns of the 4th International Conference on Modeling, Simulation and Applied Optimization (ICMSAO)*, 2011.

[12] J. M. Smith, M. P. Olivieri, A. Lackpour, and N. Hinnerschitz, "Rf-mobility gain: Concept, measurement campaign, and exploitation," *IEEE wireless communications*, vol. 16, no. 1, February 2009.

[13] M. Lindhe and K. H. Johansson, "Using robot mobility to exploit multipath fading," *IEEE wireless communications*, vol. 16, no. 1, February 2009.

[14] A. Ghaffarkhah and Y. Mostofi, "Path planning for networked robotic surveillance," *IEEE Transactions on signal processing*, vol. 60, no. 7, July 2012.

[15] Y.-H. L. H.Y. Yongguo Mei and L.C.S.G., "A case study of mobile robots energy consumption and conservation techniques," *Proceedings of 12th International Conference on Advanced Robotics, ICAR'05*, 2005.

[16] G. Caprari and R. Siegwart, "Mobile micro-robots ready to use: Alice," *Proceedings of IEEE/RSJ International Conference on Intelligent Robots and Systems, 2005. (IROS 2005)*, 2005.

[17] ——, "Mobile micro-robots ready to use: Alice," *Proceedings of IEEE/RSJ International Conference on Intelligent Robots and Systems, 2005. (IROS 2005)*, 2005.

[18] S. S. A. H. Coarasa, P. Nintanavongsa and K. Chowdhurry, "Impact of mobile transmitter sources on radio frequency wireless energy harvesting," *Proceedings of 2013 International Conference on Computing, Networking and Communications, Green Computing, Networking and Communications Symposium*, 2013.

[19] J. O. McSpadden, L. Fan, and K. Chang, "Design and experimentss of a high-conversion-efficiency 5.8-ghz rectenna," *IEEE transactions on microwave theory and techniques*, vol. 46, no. 12, December 1998.

[20] G. Caprari, T. Estier, and R. Siegwart, "Fascination of down scaling-alice the sugar cube robot," *Journal of Micromechatronics*, vol. 1, no. 3, 2002.

[21] X. Zhou, R. Zhang, and C. K. Ho, "Wireless information and power transfer: Architecture design and rate-energy tradeoff," *IEEE transactions on communications*, vol. 61, no. 11, November 2013.

[22] D. Bonilla, D. McLernon, and M. Ghogho, "Designing optimal trajectory planners for robotic communications," *Proceedings of the 1st IET Intelligent Signal Processing (ISP)*, December 2013.

[23] R. Siegwart, I. R. Nourbakhsh, and D. Scaramuzza, *Introduction to autonomous mobile robots, second edition*. MIT Press, 2011.

[24] H. Kim and B. K. Kim, "Minimum-energy trajectory planning and control on a straight line with rotation for three-wheeled omni-directional mobile robots," *Proceedings of the International Conference on Intelligent Robots and Systems*, 2012.

[25] G. Dudek and M. Jenkin, *Computational principles of mobile robotics*. Cambridge University Press, 2000.

[26] "Energy harvesting kits," *www.powercastco.com/products/*.

[27] C. H. Kim and B. K. Kim, "Minimum-energy rotational trajectory planning for differential-driven wheeled mobile robots," *Proceedings of the 13th International Conference on Advanced Robotics (ICAR)*, 2007.

[28] R. Weber, *Introduction to Microwave Circuits: Radio Frequency and Design Applications*. Wiley-IEEE Press, 2001.

[29] W. C. Jakes, *Microwave mobile communicaions*. Wiley-Interscience Publication, 1974.

[30] A. Kansal, J. Hsu, S. Zahedi, and M. B. Srivastava, "Power management in energy harvesting sensor," *ACM Transactions on Embedded Computing Systems (TECS) - Special Section LCTES'05*, vol. 6, no. 4, September 2007.

[31] M. Malmirchegini and Y. Mostofi, "On the spatial predictability of communication channels," *IEEE transactions on wireless communications*, vol. 11, no. 3, 2012.

[32] E. D. Anese, S.-J. Kim, and G. B. Giannakis, "Channel gain map tracking via distributed kriging," *IEEE transactions on vehicular technology*, vol. 60, no. 3, 2011.

[33] S. Russell and P. Norvig, *Artificial Intelligence A Modern Approach, second edition*. Prentice Hall, 2003.

[34] N. Blaustein and Y. B. Shimol, "Prediction of frequency dependence of path loss and link-budget design for various terrestrial communication links," *IEEE Transactions on Antennas and propagation*, vol. 52, no. 10, 2004.

[35] C. U. S. A. R. Moghimi, Hsin-Mu Tsai, "Characterizing intra-car wireless channels," *IEEE Transactions on Vehicular Technology*, vol. 58, no. 9, 2009.

[36] R. Dickinson, "Evaluation of a microwave high power reception-conversion array for wireless power transmission," *Jet Propulsion Laboratory, California Institute of Technology, Pasadena, CA, Tech. Memo 33-741*, September 1975.

[37] D. E. Kirk, *Optimal control theory: An introduction*. Dover Publications, Inc., 2004.

[38] F. L. Lewis and V. L. Syrmos, *Optimal control, second edition*. Wiley-Interscience Publication, 1995.

Daniel Bonilla Licea received his telematics engineering degree from the Unidad Profesional Interdisciplinaria en Ingenieria y Tecnologias Avanzadas, UPIITA, Mexico, in 2009. He received his M.Sc. degree in communications from the Centro de Investigacion y Estudios Avanzados, CINVESTAV, Mexico City, in 2011. From May 2011 until June 2012, he did an internship in the signal processing team of Intel Labs in Guadalajara, Mexico. From September 2012 to the present day he has been doing a PhD at the School of Electronics and Electrical Engineering, University of Leeds, U.K.

Syed Ali Raza Saidi (S09) received his B.Eng.degree in information and communication system engineering from the School of Electronics and Electrical Engineering, NUST, Pakistan, in 2008. He was awarded the NUST most prestigious Rectors gold medal for his nal year project. From September 2007 until August 2008, he served as a Research Assistant in the Wireless Sensor Network Lab on a collaborative research project between NUST, Pakistan, and Ajou University, South Korea. In 2008, he was awarded the overseas research student (ORS) scholarship along with the Tetley Lupton and Excellence Scholarships to pursue his Ph.D. at the School of Electronics and Electrical Engineering, University of Leeds, U.K. He was also awarded with the COSTIC0902, DAAD, and Royal Academy of Engineering grants to promote his research. His research is focused on the design and analysis of large scalead-hoc wireless networks by employing tools from stochastic geometry and random graph theory.

Des McLernon (M94) received his B.Sc in electronic and electrical engineering and his M.Sc. in electronics, both from Queens University of Belfast, N. Ireland. He then worked on radar research and development with Ferranti Ltd. in Edinburgh, Scotland, and later joined the Imperial College, University of London, where he received his Ph.D.in signal processing. After first lecturing at South Bank University, London, UK, he moved to the School of Electronic and Electrical Engineering at the University of Leeds, UK, where he is a Reader in Signal Processing and Director of Graduate Studies. His research interests are broadly within the domain of signal processing for communications, in which area he has published over 280 journal and conference papers.

Mounir Ghogho received the PhD degree in 1997 from the National Polytechnic Institute of Toulouse. Since 2001, he has been a full Professor with the EEE school of the University of Leeds (UK). Since 2010, he has also been affiliated with the International University of Rabat. He is an Associate Editor of the IEEE Signal Processing magazine. He previously served as Associate Editor of IEEE Transactions on Signal Processing. He is a member of the IEEE SAM Technical Committee. He was awarded the UK Royal Academy of Engineering Research Fellowship in 2000 and the 2013 IBM Faculty award in 2013.